

# An Integral Backstepping Algorithm for a DFIG-Based Wind Turbine Connected to the Undisturbed Utility Grid

El Mahfoud Boulaoutaq<sup>1\*</sup>, Mustapha Kourchi<sup>2</sup>, Azeddine Rachdy<sup>2</sup>

<sup>1</sup>LASIME, National School of Applied Sciences, Ibn Zohr University, Agadir, Morocco. \*elmahfoud.boulaoutaq.mahfoud@edu.ac.ma

<sup>2</sup>LASIME, Higher School of Technology of Agadir, Ibn Zohr University, Agadir, Morocco.

## Article Info

Volume 81

Page Number: 4446 - 4460

Publication Issue:

November-December 2019

## Abstract

This paper aims to model the entities of a Doubly Fed Induction Generator (DFIG) based Wind Turbine (WT), to design and then synthesize the command part using the Backstepping algorithm with integral action (IBS). The main rule of this method is to take some state variables as virtual controls, then to design an intermediate controller. It consists in controlling the BTB converters so as to master the active and reactive exchange of power with the undisturbed utility grid, and this in the case where the maximum power available in the wind is harvested (MPPT control) and also in case this harvesting is limited to the rated power conversion chain (Pitch Control). In order to evaluate the performance of the designed controller by the IBS algorithm, a series of simulations is carried in the MATLAB / SIMULINK. A comparative study with conventional PI regulators is evoked.

**Keywords:** DFIG-based WT, Back-To-Back (RSC and GSC), Integral Backstepping, MPPT by Optimal TSR, Pitch control.

## Article History

Article Received: 5 March 2019

Revised: 18 May 2019

Accepted: 24 September 2019

Publication: 23 December 2019

## I. Introduction

In recent years, traditional sources have failed to over-come the global energy need. This is due to the incessant increase in demand but especially to the rerouting of natural resources and also the new strict regulations imposed on these plants. To achieve sustainable development, the promotion of renewable energy (RE) penetration into electrical systems was considered a crucial solution [1-4]. As RE's representative, wind energy has grown the fastest and cumulative installed capacity of wind generators worldwide could exceed 800 GW by 2021 [5-6].

Among the different types of wind energy conversion systems (WECSs), those based on the doubly feed induction generator (DFIG) are widely used thus dominating the largest proportion of the market. and this thanks to their wide speed range, their independent control of active and reactive power and their lower power of the excitation converter occupies instead [6-7]. In a DFIG-based WECSs as shown in Fig. 1 [8-9], the stator is directly connected to the utility grid while the rotor is connected to the grid via a back-to-back bidirectional converter (BTB): rotor converter (RSC) and grid converter (GSC). This bidirectional BTB converter controls the appropriate amount (dictated by the wind farm supervisor) of active

and reactive power injection at the point of common coupling (PCC) while maintaining a constant DC link voltage during stationary and transient regime conditions of the WECS based on DFIG connect-ed to the utility grid [4], [7-8].

Due to their simplicities, linear control based on the sta-tor voltage-oriented control (SVOC) strategies are used to master DFIG-based WECS at its normal production or in its contribution to the systems services (e.g. frequency setting, FRT capability, ...) [9-12]. But as these control-lers are designed from linearized DFIG-base WECS models, they will eventually suffer from parametric and non-linear variations of the system and also from the change of the operating point. The DFIG-based WECS have some nonlinearities, the main ones being the varia-tions of the wind speed which are always nonlinear, the electromagnetic torque which is a nonlinear function of the rotor and stator currents [8]. Subsequently, nonlinear controllers based on different nonlinear control tech-niques are mobilized (e.g. sliding mode [13], Active Dis-turbance Rejection Control [7,14], Feedback lineariza-tion [15], Backstepping [3,16], ...) because the design process of these controllers doesn't depend on the oper-ating points.

The Sliding Mode (SM) strategy offers robustness against nonlinearities and external disturbances. In [13], the SM algorithm is used for the RSC, while a classical PI controller is employed to control GSC. Although the SM controller is robust with a quicker convergence rate, these controllers usually pose the following problem: the chattering phenomenon which could motivate the un-modeled dynamics and the choice of a generalized slid-ing surface varying in time with the wind speed profile.

In [7] and [14] the chain is controlled by a recent type of non-linear controller called Active Disturbance Rejection Control (ADRC) which gave very satisfactory results in terms of robustness especially with respect to parametric variations, but the authors of [7] were limited to com-mand only the RSC and the MPPT strategy, and in [14] the pitch control is not processed.

In [15] the DFIG-based WECS controllers are designed using feedback linearization strategy (FBL) in order to improve transient performance. For its successful im-plementation the FBL controller requires precise and accurate parametric information about the system. In addition, when designing the controller, the FBL method cancels some useful nonlinearities of the system.

The Backstepping (BS) technique uses all nonlinearities during the controller design process and thus improves system performance [7]. The basic form of BS method is used to synthesize the RSC and MPPT controllers in [3], it showed good quality of tracking, regulation and rejection of all disturbances but it suffers from a perma-nent static error during the regulation. In [16] present a BS technique to control two power converters RSC and GSC but without any interest in controlling the system for wind speeds higher than rated speed. [17] used adap-tive Backstepping method to harvest the MPP of a DFIG-based WECS. This controller avoids the wind speed sensor in the MPPT algorithm. The results visibly show the control effectiveness against the wind speed variations and parametric deviations.

Backstepping is a method that recursively constructs, in a systematic and direct way, the control law, adaptive dynamics and Lyapunov function that ensure the over-all stability of the control subject system. The Backstep-ping controller can achieve tracking and stabilization objectives because it is a recursively-based controller that divides a complete system into lower-order systems. it avoids canceling the useful non-linearities. The main idea of BS technique is to derive a controller recursively and move away from the subsystem gradually, ensuring stability for each stage until the last step [18]. various practical aspects of Backstepping are considered and changes are made to make it usable on real processes. Among these improvements are cited Backstepping with filter of unavoidable measurement noise affecting the measured quantities, and Backstepping

with integral action to cancel the effect of disturbances at zero average [16], [18-19]. The contribution of this paper is the design and testing of the nonlinear integral Backstepping method applied to the DFIG-based WECS in their two command levels. Subsequently, IBS scheme is used to design the MPPT algorithm by optimal tip speed ratio (OTSR), RSC - GSC controllers with the purpose of regulating the power at the PCC. The pitch control is provided by the classical PI controller. For these, the dynamic models of all the entities making up the system of Figure 1 are established. and through simulation tests of the designed and synthesized controllers we prove that the IBS method can increase the system robustness towards external disturbances and system parameter changes.

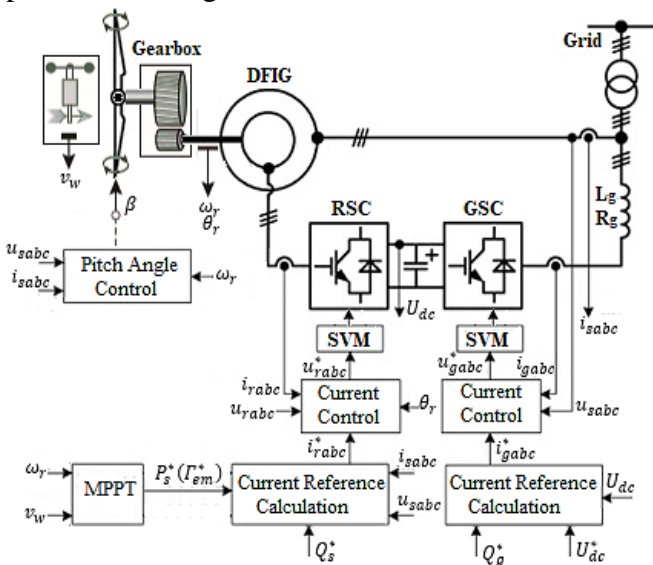


Fig 1: Wind Turbine controlled by Integral Backstepping technique.

This paper is structured in six sections: An introduction in section 1. Section 2 provides the model of DFIG-based WECS. Section 3 presents the IBS algorithm based on the Lyapunov stability technique. Section 4 presents the design of all controllers. Section 5 will be reserved to the simulation results under the MATLAB / Simulink and their interpretations. The main conclusions of this work are presented in the final section.

## II. Modeling the DFIG-based WECS

The topology of the DFIG-based WECS connected to the utility grid subject of modeling is shown in Fig1. At first, we will establish the aerodynamic model of the turbine. Then, the model of the mechanical transmission. Finally, we model the electrical part of the chain of which we will model the DFIG, the converters RSC and GSC, DC Link, and the harmonic filter.

### 1. Model of the Turbine

The wind speed  $v_w$ , applied to the blades of the wind turbine, causes its rotation and subsequently a mechanical power is created on the shaft of the turbine, noted  $P_t$ , expressed by

$$P_t = 0.5 C_p(\lambda, \beta) \rho S v_w^3 \quad (1)$$

Where  $\lambda$  is defined by:

$$\lambda = \frac{R \Omega_t}{v_w} \quad (2)$$

With  $\rho$ ,  $S$ ,  $\lambda$ ,  $\Omega_t$ , and  $R$  are the air density ( $\sim 1,225 \text{ kg/m}^3$ ), Tip Speed Ratio (TSR) which is the ratio between the linear velocity at the end of the blades and the wind speed, the surface swept by the turbine, Turbine rotation speed, and the turbine radius or the blade length, respectively.

The  $C_p$  values are usually provided by the manufacturers and deduced from the experimental tests. In the literature, numerous analytic formulas are used for its approximation [20-21]. In this paper, the  $C_p$  is expressed as follows:

$$C_p(\lambda, \beta) = 0,5 \left( \frac{116}{\lambda_i} - 0,4\beta - 5 \right) e^{-\frac{21}{\lambda_i}} \quad (3)$$

With  $\lambda_i = \frac{1}{\lambda + 0,08\beta} - \frac{0,035}{1 + \beta^3}$ , and  $\beta$  is the blades pitch angle.

The mechanical torque  $\Gamma_t$  developed on the slow shaft of the turbine is expressed:

$$\Gamma_t = \frac{P_t}{\Omega_t} = 0,5 \cdot \frac{\pi}{\lambda} \cdot \rho \cdot R^3 \cdot v_w^2 \cdot C_p(\lambda, \beta) \quad (5)$$

Fig 2 shows the  $C_p$  progression as a function of  $\beta$  and  $\lambda$ .

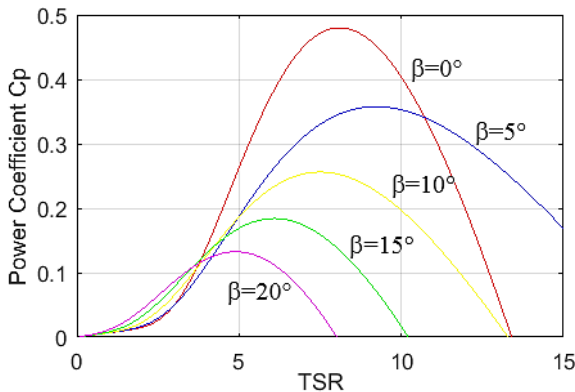


Fig 2:  $C_p$  Evolution for different  $\beta$  and TSR

## 2. Model of the mechanical part

Three blades of length  $R$ , identical and orientable constitute the aerodynamic part of the turbine. They are fixed on a hub integral with a drive shaft rotating at  $\Omega_t$ . The latter is connected to a gain multiplier  $G$  which restores its mechanical energy to the DFIG. In addition, we consider that the wind speed is uniformly distributed on all blades, so all thrust forces are equal. Thus, the three blades are modeled as a single mechanical system with its characteristics is the sum of the mechanical characteristics of each of them. Due to the blades aerodynamic design, we consider that their friction coefficient with respect to the air is neglected. Similarly, the turbine speed being so low that the friction losses will be negligible in the generator sider. Based on these assumptions, we obtain a model shown in Figure 3 which is a two-mass model. in [22], the validity of the latter has been verified by comparing it with the complete model of the turbine

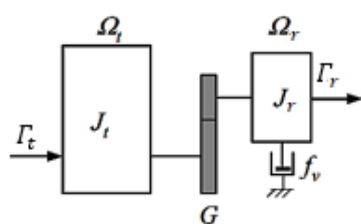


Fig 3: Turbine mechanical model

Where  $J_b$ ,  $J_r$ ,  $f_v$ ,  $\Gamma_r$ ,  $\Omega_r$  are the inertia moment of the turbine, the inertia moment of the DFIG, the viscous friction coefficient of the DFIG, the mechanical torque on the fast shaft, the DFIG rotation speed respectively.

The multiplier adjusts the turbine speed (slow shaft) to the DFIG speed (fast shaft). by neglecting the losses of the multiplier, we can model it as follows:

$$\begin{cases} \Gamma_r = \frac{\Gamma_t}{G} \\ \Omega_r = G\Omega_t \end{cases} \quad (6)$$

From the Fig 3, and by bringing the whole to rapid speed shaft, we can write the dynamics fundamental equation of the system as follows:

$$\Gamma_r = J\dot{\Omega}_r + f_v\Omega_r + \Gamma_{em} \quad (7)$$

With  $J = \frac{J_t}{G^2} + J_r$ , and  $\Gamma_{em}$  is the DFIG electromagnetic torque.

Using per unit (pu) form, Equation (7) could be written as:

$$\Gamma_r = 2H\dot{\Omega}_r + f_{v-pu}\Omega_r + \Gamma_{em} \quad (8)$$

where  $H = \frac{J \cdot \omega_B^2}{2 \cdot S_B \cdot p^2}$  (in s), and  $f_{v-pu} = \frac{f_v \cdot \omega_B^2}{S_B \cdot p^2}$ .  $S_B$  (in VA),  $\omega_B$  (in rd/s) and  $p$  are the total inertia, the generator base apparent power, the generator base angular frequency and the generator number of pole pairs respectively.

The synoptic of Fig 4 displays the aerodynamic and mechanical part models of the WECS. It shows that DFIG speed  $\Omega_r$ , and therefore  $\Omega_t$ , could be mastered by acting either on the DFIG electromagnetic torque  $\Gamma_{em}$  (MPPT algorithm) or on the pitch angle  $\beta$  (Pitch Control). Wind speed  $v_w$  is considered a disturbance input.



Applying Park's transformation, Eq. (15) become as follows:

$$\begin{cases} v_{rdq} = S_{rdq} U_{dc} \\ v_{gdq} = S_{gdq} U_{dc} \end{cases} \quad (15)$$

This Converter can operate as inverter or rectifier.

### 5. DC Link and harmonic filter Modeling.

A harmonic filter is set up to interconnect the GSC to the PCC. It is a series  $L_g - R_g$  filter as illustrated in Fig. 1. Indq-axis reference, it's modeled in pu by the following equation:

$$\begin{aligned} v_{gd} &= -R_g i_{gd} - L_g w_B^{-1} \dot{i}_{gd} + L_g i_{gq} + v_{sd} \\ v_{gq} &= -R_g i_{gq} - L_g w_B^{-1} \dot{i}_{gq} - L_g i_{gd} + v_{sq} \end{aligned} \quad (16)$$

The power balance at the DC link is  $P_C = |P_g - P_r|$ . In pu, this equation becomes:

$$C U_{dc} \dot{U}_{dc} = w_B \cdot (P_g - P_r) \quad (17)$$

Equation (18) can be write in the linear form

$$\dot{w} = \frac{2}{C} w_B \cdot (P_g - P_r) \quad (18)$$

Where  $w = U_{DC}^2$

### III. Backstepping Technique Concept

The central idea of Backstepping is to recursively derive a controller and step back from the subsystem gradually, guaranteeing stability for each step, until getting to the last step [18].

Backstepping is based on the second method of Lyapunov, which combines the choice of the function with that of the laws of control and adaptation. This allows him, in addition to the duty for which the controller is designed (tracking and / or regulation), to guarantee, at all times, the overall stability of the compensated system [3], [21].

various practical aspects of Backstepping are considered and changes are made to make it usable on real pro-cesses. Among these improvements are cited Backstep-ping with filter of unavoidable measurement noise af-fecting the measured quantities, and Backstepping with integral action to

cancel the effect of disturbances at zero average [16], [18-19].

To simplify the presentation, the method is developed on linear systems. Its extension to non-linear systems is straightforward and requires no major modification. The transfer function of the linear process to be controlled is given by:

$$G(s) = \frac{K}{\tau s + 1} \quad (19)$$

Which corresponds, in the time domain, to the differential equation

$$\dot{y}(t) + \frac{1}{\tau} y(t) = \frac{K}{\tau} u(t) \quad (20)$$

Instead of using this last equation in the design procedure, it is replaced by its derivative. This gives as new equation

$$\ddot{y}(t) + \frac{1}{\tau} \dot{y}(t) = \frac{K}{\tau} \dot{u}(t) \triangleq v(t) \quad (21)$$

The choise

$$\begin{cases} x_1 = y(t) \\ x_2 = \dot{y}(t) \end{cases} \quad (22)$$

Gives as state representation of the system

$$\begin{cases} \dot{x}_1 = x_2 \\ \dot{x}_2 = -\frac{1}{\tau} x_2 + v \end{cases} \quad (23)$$

▪ **Step 1** - The first error variable is always defined by

$$\varepsilon_1 = y - y_r = x_1 - y_r \quad (24)$$

Where,  $y_r$  is the reference trajectory to follow.

If we take as control function of Lyapunov (**cf**)

$$V_1(\varepsilon_1) = \frac{1}{2} \varepsilon_1^2 \quad (25)$$

Its derivative will be given by

$$\dot{V}_1 = \varepsilon_1 \dot{\varepsilon}_1 = \varepsilon_1 [x_2 - \dot{y}_r] \quad (26)$$

To make it negative, just take

$$(x_2)_d \triangleq \alpha_1 = -k_1 \varepsilon_1 + \dot{y}_r \quad (27)$$

Where  $k_1 > 0$  is a design parameter

▪ **Step 2** - We define the new error variable

$$\varepsilon_2 = x_2 - \alpha_1 = x_2 + k_1 \varepsilon_1 - \dot{y}_r \quad (28)$$

And the cfl

$$V_2 = \frac{1}{2} \varepsilon_1^2 + \frac{1}{2} \varepsilon_2^2 \quad (29)$$

Its derivative, along the system's trajectories, is given by

$$\begin{aligned} \dot{V}_2 &= -k_1 \varepsilon_1^2 + \varepsilon_2 [\dot{\varepsilon}_2 + \varepsilon_1] \\ &= -k_1 \varepsilon_1^2 + \varepsilon_2 \left[ -\frac{1}{\tau} x_2 + v - \ddot{y}_r \right. \\ &\quad \left. + (1 - k_1^2) \varepsilon_1 + k_1 \varepsilon_2 \right] \end{aligned} \quad (30)$$

To make it negative, we should take

$$v = \frac{1}{\tau} x_2 + \ddot{y}_r - (1 - k_1^2) \varepsilon_1 - (k_1 + k_2) \varepsilon_2 \quad (31)$$

Where  $k_2 > 0$  is a design parameter

A simple integration makes it possible to obtain as final order

$$u = \frac{\tau}{K} \cdot \frac{v}{s} \quad (32)$$

The application of this last command to the system of equation (20) returns the results of the Fig. 6 (a) and (b). These show a comparison between the Integral Backstepping version and the basic Backstepping version which the system is subjected to a disturbance at the output which appears at time 1s and lasts 2s. The pursuit behaviors are very similar, whereas in regulation the Integral Backstepping ensures, contrary to the basic Backstepping, a null error in steady state. All this is achieved through gentle excitement.

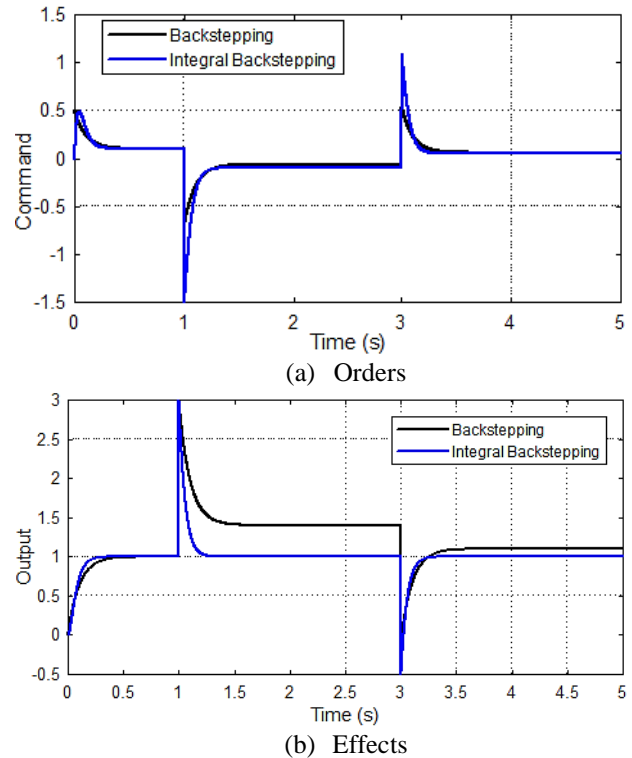


Fig 6: Disturbance in echelon: Backstepping with vs without integrator

#### IV. Regulators Design

In this section, we will synthesize the controllers, by Integral Backstepping algorithm, of our DFIG-based WECS. To do this, we will rewrite the model of our system in the canonical form of design by Backstepping Technique, and then we design the regulators controlling the MPPT, the Pitch Angle, and the BTB converters RSC and GSC.

##### 1. MPPT Regulator

As the wind speed is a random quantity, the efficiency of the energy conversion of the WECS is increased by extracting the maximum power available in the wind. For a given wind speed value, the MPPT strategy goes to find the maximum power from the kinetic energy of the wind. The working region of the MPPT control corresponds to the wind speeds lower than the nominal wind speed. Many MPPT control methods have been studied in literature and applied in the WECS industry [3], [8], [9]. These methods determine  $\omega_r^*$ ,  $\Gamma_{em}^*$ , or  $P_s^*$ ; reference of DFIG speed, electromagnetic torque, or DFIG power,

respectively. The interested reader will find a comparative table between these techniques at [9], it indicates that optimal tip speed ratio (OTSR) strategy it combines the simplicity of its structure and the good control performance.

The MPPT with OTSR is shown in Fig. 8. This algorithm offers DFIG speed reference  $\omega_r^*$  based on the measured wind speed  $v_w$ .  $\omega_r^*$  is attuned in proportion to  $v_w$ , so that the WECS always works at the  $\lambda_{opt}$  value to achieve the maximum power point. This tuning is established as follows based on the expression of TSR (2):

$$\begin{aligned} \Omega_r^* &= G\Omega_t^* = \frac{\lambda_{opt} G}{R} v_w \\ &= K_{Opt} v_w \end{aligned} \quad (33)$$

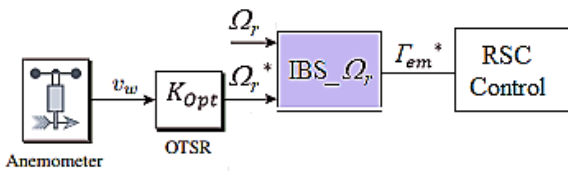


Fig 7: MPPT by Optimal TSR (OTSR)

**Note:** Since the new ultrasonic sensors provide more reliable and truthful wind speed information, they are promising for this MPPT algorithm.

The design of the regulator mastering the speed of the MADA is based on the equation (8) that one writes in the canonical form to apply the technique of Backstepping.

Deriving the expression (8), we obtain:

$$\dot{\Gamma}_r = 2H\ddot{\Omega}_r + f_{v-pu}\dot{\Omega}_r + \dot{\Gamma}_{em} \quad (34)$$

Let,

$$\begin{cases} x_1 = \Omega_r \\ x_2 = \dot{x}_1 \end{cases} \quad (35)$$

This gives as new state representation of the system (34)

$$\begin{cases} \dot{x}_1 = x_2 \\ \dot{x}_2 = \frac{1}{2H}(\dot{\Gamma}_r - \Gamma_{em\_c} - f_{v-pu}x_2) \end{cases} \quad (36)$$

Consider the error variables

$$\varepsilon_1 = x_{1ref} - x_1 \quad (37)$$

$$\varepsilon_2 = x_{2ref} - x_2$$

Recursive design application by IBS gives for the virtual order

$$x_{2ref} = \dot{x}_{1ref} + k_{\Omega 1}\varepsilon_1 \quad (38)$$

And the real command

$$\begin{aligned} \Gamma_{em}^* &= \frac{-1}{s}(2H(\dot{x}_{1ref} + (1 - k_1^2)\varepsilon_1 \\ &\quad + (k_1 + k_2)\varepsilon_2) + f x_2 - \dot{\Gamma}_r) \end{aligned} \quad (39)$$

$k_{\Omega 1}, k_{\Omega 2}$  are the positive setting parameters.

## 2. RSC Regulators Design

Due to no disruptions of the utility grid in our case, we choose the dq-axis related to the stator rotating field SVOC and neglecting the resistance of the stator windings, and from equations (10) and (11). The state representation chosen for the rotor side converter control is:

$$\dot{i}_{rd} = \frac{W_B}{\sigma L_r}(v_{rd} - R_r i_{rd} + \sigma L_r(1 - \omega_r)i_{rq}) \quad (40)$$

$$\begin{aligned} \dot{i}_{rq} &= \frac{W_B}{\sigma L_r}(v_{rq} - R_r i_{rq} - \sigma L_r(1 - \omega_r)i_{rd} \\ &\quad - (1 - \omega_r)\frac{L_m}{L_s}\varphi_s) \end{aligned} \quad (41)$$

The setpoints of these currents are deduced from the setpoints of the active power (or electromagnetic torque) and the reactive power as follows:

$$\Gamma_{em}^* = -1.5p\frac{L_m}{L_s}\varphi_{sd}i_{rq}^* \quad (42)$$

$$Q_s^* = 1.5\left(\frac{v_{sq}^2}{L_s W_s} - v_{sq}\frac{L_m}{L_s}i_{rd}^*\right) \quad (43)$$

Deriving the expression (41), we obtain:

$$\begin{aligned} \dot{v}_{rq} = & \sigma L_r w_B^{-1} \dot{i}_{rq} + R_r i_{rq} \\ & + \sigma L_r (1 - \omega_r) i_{rd} + (1 \\ & - \omega_r) \frac{L_m}{L_s} \dot{\phi}_s \triangleq u_{rq} \end{aligned} \quad (44)$$

Let,

$$\begin{cases} x_3 = i_{rq} \\ x_4 = \dot{x}_4 \end{cases} \quad (45)$$

This gives as new state representation of the system (39)

$$\begin{cases} \dot{x}_3 = x_4 \\ \dot{x}_4 = \frac{1}{\sigma L_r w_B^{-1}} (u_{rq} - R_r x_2 - \sigma L_r (1 - \omega_r) i_{rd} \\ - (1 - \omega_r) \frac{L_m}{L_s} \dot{\phi}_s) \end{cases} \quad (46)$$

Consider the error variables

$$\varepsilon_3 = x_{3ref} - x_3 \quad (47)$$

$$\varepsilon_3 = x_{4ref} - x_4$$

Recursive design application by Backstepping gives for virtual control

$$x_{4ref} = \dot{x}_{3ref} + k_{rq1} \varepsilon_3 \quad (48)$$

And for the real order

$$\begin{aligned} v_{rq} = & \frac{\sigma L_r}{w_B S} (\ddot{x}_{1ref} + (1 - k_{rq1}^2) \varepsilon_3 \\ & + (k_{rq1} + k_{rq2}) \varepsilon_4 + \frac{R_r w_B}{\sigma L_r} x_4 \\ & + (1 - \omega_r) [x_6 + \frac{L_m}{L_s \sigma L_r}] \dot{\phi}_s) \end{aligned} \quad (49)$$

$k_{rq1}, k_{rq2}$  are positive setting parameters.

Applying the same design to the system(40) and choosing

$$\begin{cases} x_5 = i_{rd} \\ x_6 = \dot{x}_3 \end{cases} \quad (50)$$

The virtual command is

$$x_{6ref} = \dot{x}_{5ref} + k_{rd1} \varepsilon_5 \quad (51)$$

And the real command

$$\begin{aligned} v_{rd} = & \frac{\sigma L_r}{w_B S} (\ddot{x}_{5ref} + (1 - k_{rd1}^2) \varepsilon_5 \\ & + (k_{rd1} + k_{rd2}) \varepsilon_6 \\ & + \frac{w_B R_r}{\sigma L_r} x_6 - x_4 (1 - \omega_r)) \end{aligned} \quad (52)$$

Where  $k_{rd1}, k_{rd2}$  are positive setting parameters,  $\varepsilon_5 = \dot{i}_{rdref} - i_{rd}$ , and  $\varepsilon_6 = \dot{\varepsilon}_5$ .

Fig 8 shows the entities of the RSC control part by IBS. In addition to the IBS block restoring the command, the attracting block is the SVPWM (Space Vector Width Pulse); it's a procedure used to determine the pulse-width modulated signals for the RSC or GSC switches to generate the desired three-phase voltages for the rotor.

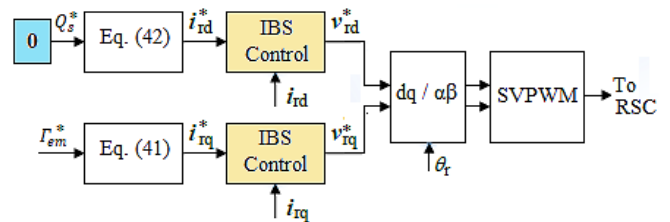


Fig 8: Regulator IBS of the RSC

### 3. GSC Regulators Design

Differentiating the expression (19) we get:

$$\dot{w} = \frac{2}{C} \left( \frac{3}{2} V_{sq} \dot{i}_{gq} - \dot{P}_{ond} \right) \quad (53)$$

Let  $x_7 = w$  and  $x_8 = \dot{w}$

This gives as new state representation

$$\begin{cases} \dot{x}_7 = x_8 \\ \dot{x}_8 = \frac{2}{C} \left( \frac{3}{2} V_{sq} \dot{i}_{gq} - \dot{P}_{ond} \right) \end{cases} \quad (54)$$

Consider the error variables

$$\begin{cases} \varepsilon_7 = x_{7ref} - x_7 \\ \varepsilon_8 = x_{8ref} - x_8 \end{cases} \quad (55)$$

The application of recursive design by Backstepping provides for virtual control

$$x_{8ref} = \dot{x}_{7ref} + k_{dc1}\varepsilon_7 \quad (56)$$

And the real control

$$i_{gq} = \frac{1}{s} \frac{C}{3V_{sq}} (\ddot{x}_{7ref} + (1 - k_{dc1}^2)\varepsilon_7 + (k_{dc1} + k_{dc2})\varepsilon_8 + \frac{2}{C}\dot{P}_{ond}) \quad (57)$$

$k_{dc1}, k_{dc2}$  are positive setting parameters.

Applying the same design to the system (16) and choosing

$$\begin{cases} x_9 = i_{gd} \\ x_{10} = \dot{x}_9 \\ x_{11} = i_{gq} \\ x_{12} = \dot{x}_{11} \end{cases} \text{ and } \begin{cases} \varepsilon_9 = x_{9ref} - x_9 \\ \varepsilon_{10} = x_{10ref} - x_{10} \\ \varepsilon_{11} = x_{11ref} - x_{11} \\ \varepsilon_{12} = x_{12ref} - x_{12} \end{cases} \quad (58)$$

Virtual commands are

$$x_{10ref} = \dot{x}_{9ref} + k_{gd1}\varepsilon_9 \quad (59)$$

$$x_{12ref} = \dot{x}_{11ref} + k_{gq1}\varepsilon_{11} \quad (60)$$

And the real orders

$$v_{gd} = \frac{L_g}{\omega_B} \left( -\dot{x}_{9ref} - (1 - k_{gd1}^2) \frac{\varepsilon_9}{s} - (k_{gd1} + k_{gd2})\varepsilon_9 \right) - R_g x_9 + L_g x_{11} \quad (61)$$

$$v_{gq} = \frac{L_g}{\omega_B} \left( -\dot{x}_{11ref} - (1 - k_{gq1}^2) \frac{\varepsilon_{11}}{s} - (k_{gq1} + k_{gq2})\varepsilon_{11} \right) - R_g x_{11} + L_g x_9 + v_{sq} \quad (62)$$

Where  $k_{gd1}, k_{gd2}, k_{gq1}, k_{gq2}$  are positive setting parameters.

Figure 9 shows the entities of the GSC control part by IBS. It regulates the DC bus voltage and contributes reactive power supplied to the utility grid.

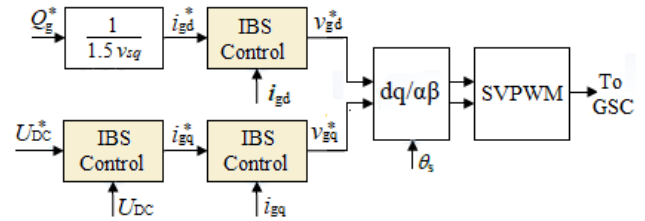


Fig 9: Regulator IBS of the GSC

#### 4. Pitch Control Design

The wind speed is random, gusts of wind can then damage the wind energy system of energy conversion, it is then necessary to limit the power converted by increasing blade pitch angle  $\beta$ . During this operation, the generator speed is controlled not to exceed its nominal rotation speed and the DFIG power is limited to its rated power. This type of control is known as the "Pitch Control". Several techniques are discussed in the literature for the design of this controller [14], [24], [25].

Fig. 10 shows the topology used in this paper to master the angle  $\beta$ , where  $\tau_\beta$  is the time constant of the blades orientation system actuator. The pitch angle regulation range and the pitch angle rate limiter are set to  $0^\circ - 60^\circ$  and  $\pm 10^\circ/s$ , respectively.

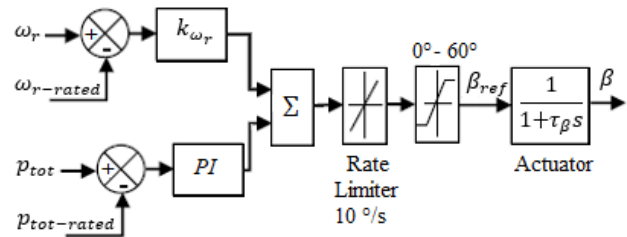


Fig 10: Pitch control Topology

#### V. Results and Interpretations

In order to validate the commands designed in the last section, simulations were performed with MATLAB Simulink. The various mechanical and electrical characteristics of the WECS subject of study are presented in Table 1. Of the latter we infer Table 2, which shows The base values used for modeling in per unit of the WECS. Table 3 shows the various adjustment parameters of the controllers designed in the last section, their values are usually obtained by the trial and error method.

Table I: Mechanical and electrical parameters of the studied WECS [9]

Entity	Parameters
Turbine	Number of blades : 3 R=45 m $J_t=1,4 \cdot 10^6$ kg.m <sup>2</sup> $v_{wt}=13$ m/s , $N_m=19$ tr/min
Gearbox	G = 100
DFIG	$P_n = 3$ MW, $U_s = 690$ V, $f = 50$ Hz, $p=2$ $R_s = 2,97$ m $\Omega$ , $R_r = 3,82$ m $\Omega$ $L_s = 121$ $\mu$ H, $L_r = 57,8$ $\mu$ H, $L_s = 12,2$ $\mu$ H $J_m = 114$ kg.m <sup>2</sup>
Utility Grid	$U_s = 690$ V, $f = 50$ Hz

Table II: Base Values

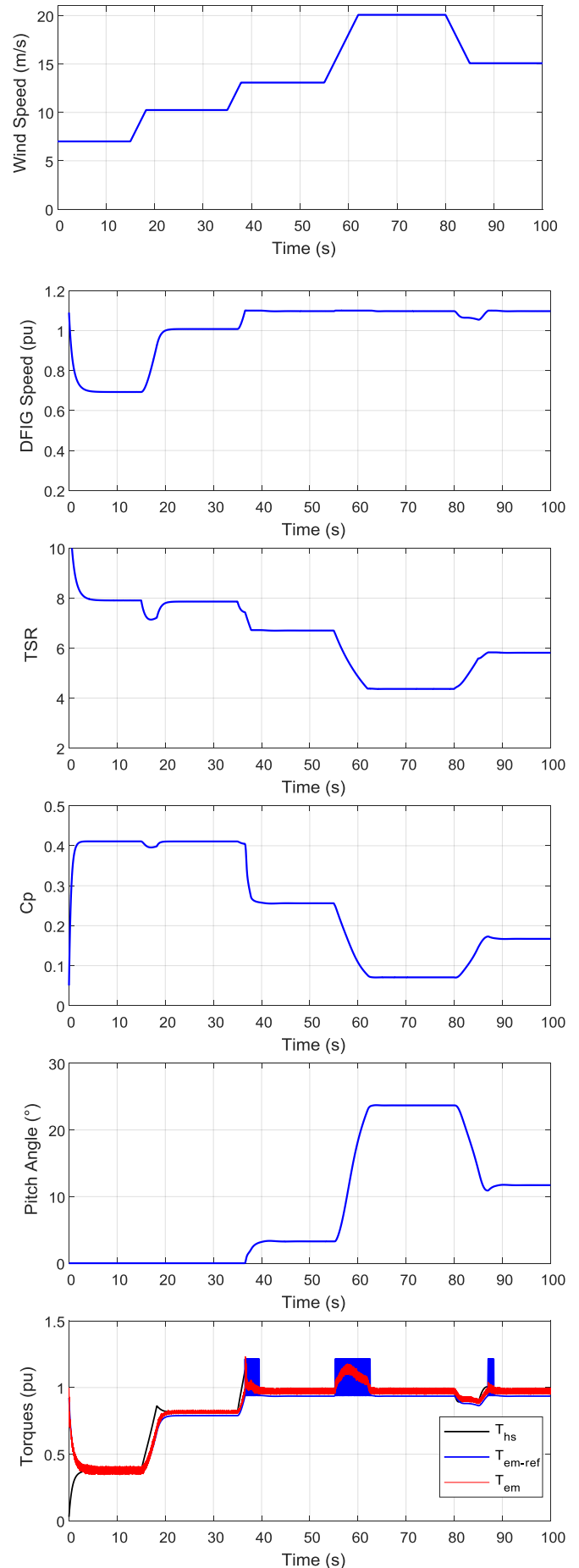
Components	Rating values
$S_B$	3 MVA
$V_B$	398,4 V
$I_B$	2510,2 A
$Z_B$	0,159 $\Omega$
$\omega_B$	314,159 rd/s
$L_B$	0,421 mH
$C_B$	16,714 mF
$\Psi_B$	1,057 Wb (rms)

Table III: Regulator Adjustment Parameters

Regulator of	Parameters
$w_r$	$k_{\Omega 1} = 10^3$ , $k_{\Omega 2} = 100$
$I_r$	$k_{rq1} = 50$ , $k_{rq2} = 10$ , $k_{rd1} = 4.5 \cdot 10^4$ , $k_{rd2} = 10^5$
$U_{dc}$	$k_{dc1} = 5$ , $k_{dc2} = 1$
$I_g$	$k_{gq1} = 0.5$ , $k_{gq2} = 10$ , $k_{gd1} = 10^3$ , $k_{gd2} = 10^6$
$\beta$	$k_{wr} = 250$ , $k_{\beta I} = 7.5$ , $k_{\beta P} = 0.75$

## 1. Results

The results obtained for the different simulation tests, are exposed on Figure 11 for tracking and regulation tests for all operation modes of our WECS, and Figure 12 for the comparison tests of the control part designed with the classical control by PI and this in terms of tracking / regulation but especially in terms of internal and external disturbance rejection, we also zoom in the control input.;



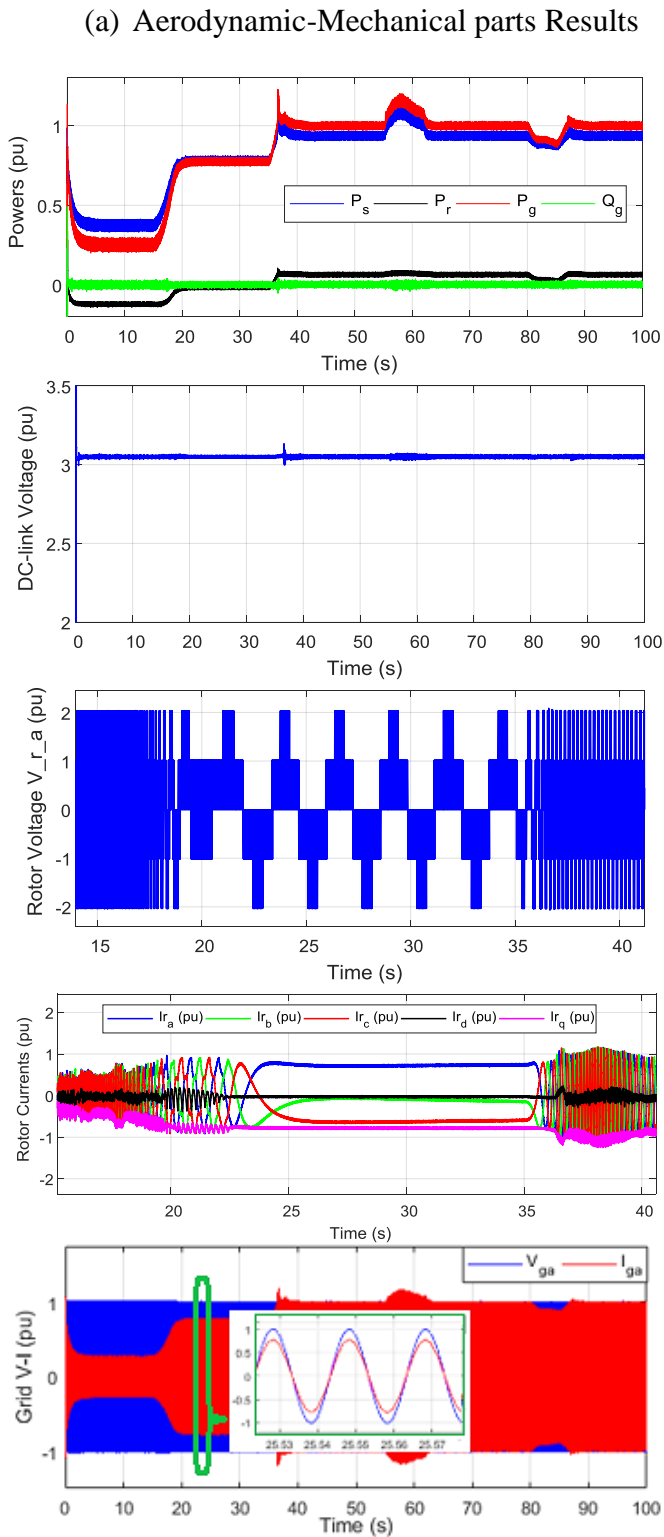


Fig 11: Tracking and regulation tests by IBS

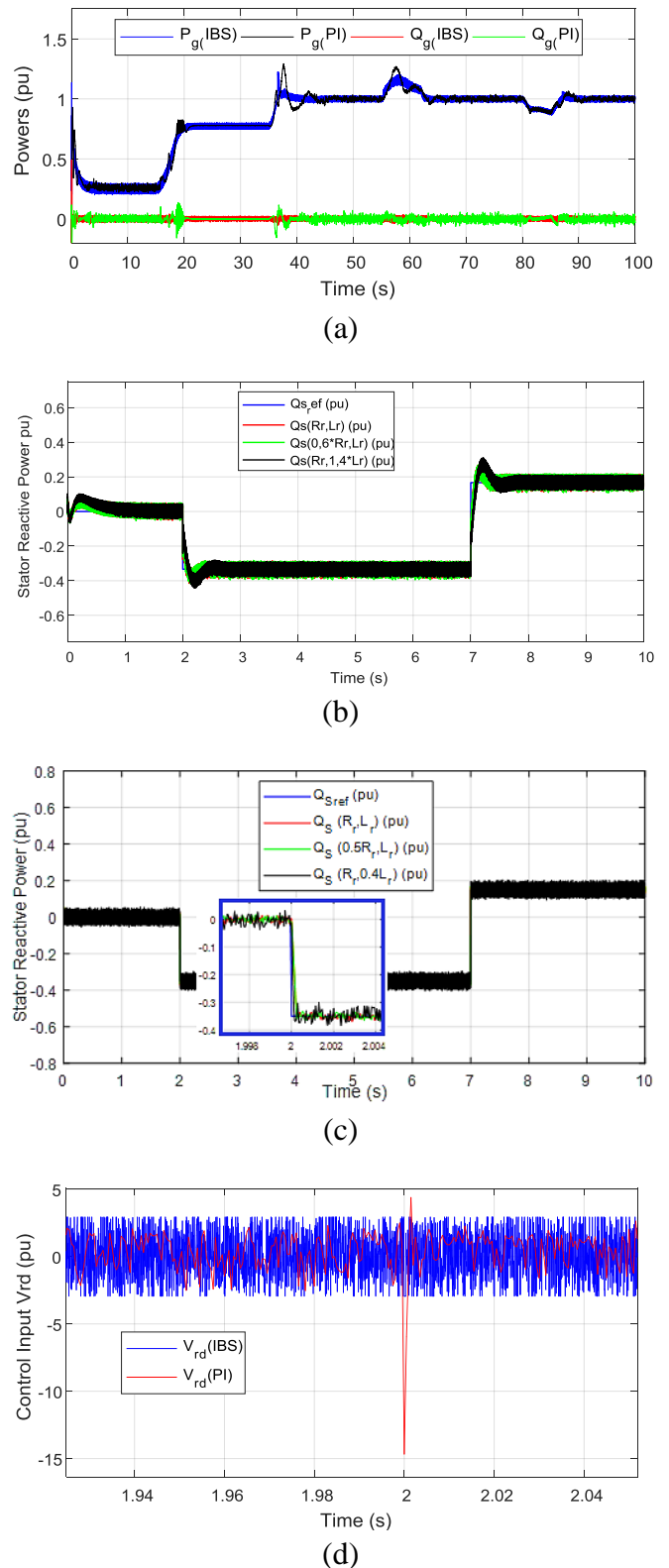


Fig 12: IBS vs PI: (a) Tracking and regulation, (b)PI robustnesstest,(c)IBS robustness test, (d) Input control  $V_{rd-ref}$

## 2. Interpretations

Figure 10 (a) shows the profiles of the aerodynamic and mechanical quantities. The wind

velocity profile applied to our WECS will make it possible to explore all the operating phases of the system and will then seek out the synthesized control algorithms; MPPT and Pitch control. This profile is divided into three areas: (i) *Hyposynchronous* where  $v_w = 7$  m/s, the DFIG rotates at  $0.7pu$ , (ii) *synchronous* where  $v_w = 10$  m/s and  $w_r = 1pu$ . For these two cases,  $C_p$  maintains its optimal value  $C_{pmax} = 0.42$  and this by requesting the MPPT by OTSR imposing a speed  $w_r$  which maintains TSR at its optimal value and thereafter the regulator imposes the electromagnetic torque adequate to recover the maximum available power. (iii) *hypersynchronous* where  $w_r > 1 pu$ ; in this zone the pitch control is biased when  $v_w$  is greater than its nominal speed ( $\sim 13m / s$ ). In the evolution of the angle  $\beta$  as a function of  $v_w$ , the impact of this variation of  $\beta$  is identified on the profile of  $C_p$  undergoing a pronounced decrease in its value and subsequently a limitation of the different mechanical quantities to their nominal values  $\Gamma_{em} = 1pu$  and also maintain  $w_r$  at its maximum value ( $\sim 1.1 pu$  in our case).

Figure 10 (b) displays the electrical quantities profiles which are only an effect of the mechanical quantities received by the DFIG. The DFIG stator power profile that tracks the speed of the wind at low speeds using MPPT and a nominal power limitation for high wind speeds thanks to Pitch Control. It also identifies the power involved in the DFIG rotor, its profile indicates that this power is bidirectional between the rotor and the network; in hyposynchrony and synchronism, it is negative and in hypersynchrony, it is positive, that is to say from the rotor towards the network. The total reactive power profile produced which is the sum of the DFIG stator reactive power and the GSC. It is noted that all of these power remains at zero. The DC bus voltage is well regulated with its  $3.05pu$  setpoint despite the various external disturbances.

The Figure 10 (b) shows also the voltage profiles from the SVPWM controlled RSC. It is noted that the frequency of these voltages depends on the slip of the mechanical frequency and the frequency of the grid, the amplitude of the tensions is at 2 levels  $\pm \frac{U_{DC}}{3}$  and  $\pm \frac{2U_{DC}}{3}$ . on the rotor these voltages

generate the currents, their frequencies vary according to the wind speed, it is noted that it is zero (of the continuous) during the phase of synchronism. The amplitude of these currents depends on  $i_{rq}$  and subsequently on the reference electromagnetic torque by the MPPT and the pitch control. The profile of the current flow in the first phase of the utility grid is also presented on the same Figure, its frequency 50 Hz is that of the grid, its amplitude depends on power output in the grid, and its phase with the voltage of the same phase is zero because the reactive power is zero.

The purpose of Figure 11 is to present a comparative study of the behavior of our system when ordered by IBS and in the case where it is ordered by the classical PI. The robustness test with respect to external disturbances ( $v_w$  for example) shows a slight superiority of the IBS algorithm as shown in Figure 11 (a). On Figure 11 (b) we find that the PI controller finds it hard to reject the internal disturbances (here variation of  $R_r$  and  $L_r$ ) whereas the IBS, by its adaptive nature, does it perfectly and this with a gentle control (figure 11 (c)).

According to these different tests we can announce that despite the problem of setting their parameters, the nonlinear IBS technical can one of the best candidates to control the DFIG-based WECS

## VI. Conclusions and Perspectives

In this paper, we modeled the diverse WECS entities. Then we applied the non-linear Integral Backstepping algorithm to control the DFIG-based WECS to produce active and reactive powers to the power grid. The chain is controlled so collect the maximum power available in the wind for wind speeds lower than the nominal (MPPT contro), and limit this harvest to the nominal power for high wind speeds (Pitch angle Control). Afterwards, we evaluated the performance of said control in tracking, regulation and robustness. The simulation results presented confirm the feasibility of the proposed control scheme, and we deduce that in addition to ensuring system stability and no convergence errors (tracking and / or regulation), IBS method offers the means to improve the quality of the transitional regime of this convergence.

**REFERENCES**

- [1] Liao, S., Yao, W., Han, X., Wen, J., & Cheng, S. (2017). Chronological operation simulation framework for regional power system under high penetration of renewable energy using meteorological data. *Applied Energy*, 203, 816-828.
- [2] Liu, J., Yao, W., Wen, J., Fang, J., Jiang, L., He, H., & Cheng, S. J. (2019). Impact of Power Grid Strength and PLL Parameters on Stability of Grid-Connected DFIG Wind Farm. *IEEE Transactions on Sustainable Energy*.
- [3] Boulaoutaq EM.; Kourchi M.; Rachdy A. (2019) Nonlinear Backstepping controller Design for Recovering the Available Maximum Wind Power by a Wind Energy Conversion System at its Partial Load. *Applied Journal of Environmental Engineering Science*, vol. 5, no 3, p. 5-3, 302-320.
- [4] Yang, C., Yang, X., & Shardt, Y. (2018). An ADRC-based control strategy for FRT improvement of wind power generation with a doubly-fed induction generator. *Energies*, 11(5), 1150.
- [5] Yang, B., Zhang, X., Yu, T., Shu, H., & Fang, Z. (2017). Grouped grey wolf optimizer for maximum power point tracking of doubly-fed induction generator-based wind turbine. *Energy conversion and management*, 133, 427-443.
- [6] Zhang, D., Xu, H., Qiao, L., & Chen, L. (2019). LVRT capability enhancement of DFIG based wind turbine with coordination control of dynamic voltage restorer and inductive fault current limiter. *PloS one*, 14(8).
- [7] Roy, T. K., Mahmud, M. A., & Oo, A. M. T. (2018, August). Nonlinear backstepping controller design for improving fault ride through capabilities of DFIG-based wind farms. In 2018 IEEE Power & Energy Society General Meeting (PESGM) (pp. 1-5). IEEE.
- [8] Boulaoutaq M., Kourchi, M., & Rachdy, A. (2019, July). Nonlinear ADRC Applied on Wind Turbine Based on DFIG Operating at its Partial Load. In 2019 International Conference of Computer Science and Renewable Energies (ICCSRE) (pp. 1-8). IEEE.
- [9] Yaramasu, V., & Wu, B. (2017). Model predictive control of wind energy conversion systems (Vol. 55). John Wiley & Sons.
- [10] Muller, S., Deicke, M., & De Doncker, R. W. (2002). Doubly fed induction generator systems for wind turbines. *IEEE Industry applications magazine*, 8(3), 26-33.
- [11] Abad, G., Lopez, J., Rodriguez, M., Marroyo, L., & Iwanski, G. (2011). Doubly fed induction machine: modeling and control for wind energy generation (Vol. 85). John Wiley & Sons.
- [12] Nian, H., & Song, Y. (2013). Direct power control of doubly fed induction generator under distorted grid voltage. *IEEE Transactions on Power Electronics*, 29(2), 894-905.
- [13] Xiong, L., Wang, J., Mi, X., & Khan, M. W. (2017). Fractional order sliding mode based direct power control of grid-connected DFIG. *IEEE Transactions on Power Systems*, 33(3), 3087-3096.
- [14] Boukhriss, A., Essadki, A., Bouallouch, A., & Nasser, T. (2014, November). Maximization of generated power from wind energy conversion systems using a doubly fed induction generator with active disturbance rejection control. In 2014 Second World Conference on Complex Systems (WCCS) (pp. 330-335). IEEE.
- [15] Chowdhury, M. A., Mahmud, M. A., Shen, W., & Pota, H. R. (2017). Nonlinear controller design for series-compensated DFIG-Based wind farms to mitigate subsynchronous control interaction. *IEEE Transactions on Energy Conversion*, 32(2), 707-719.
- [16] Bossoufi, B., Karim, M., Lagrioui, A., Taoussi, M., & ElHafyani, M. L. (2014). Backstepping control of DFIG generators for wide-range variable-speed wind turbines. *International Journal of Automation and Control*, 8(2), 122-140.
- [17] Rezaei, M. M. (2018). A nonlinear maximum power point tracking technique for DFIG-based wind energy conversion systems. *Engineering science and technology, an international journal*, 21(5), 901-908.
- [18] Fang, Y., & Fei, J. (2019). Adaptive Backstepping Current Control of Active Power Filter Using Neural Compensator. *Mathematical Problems in Engineering*, 2019.

- [19] Xiong, P., & Sun, D. (2015). Backstepping-based DPC strategy of a wind turbine-driven DFIG under normal and harmonic grid voltage. *IEEE Transactions on Power Electronics*, 31(6), 4216-4225.
- [20] El Azzaoui, M., Mahmoudi, H., & Ed-dahmani, C. (2016, May). Backstepping control of a Doubly Fed Induction Generator integrated to wind power system. In *2016 International Conference on Electrical and Information Technologies (ICEIT)* (pp. 306-311). IEEE.
- [21] Reddak, M., Berdai, A., Gourma, A., & Belfqih, A. (2016, May). Integral backstepping control based maximum power point tracking strategy for wind turbine systems driven DFIG. In *2016 International Conference on Electrical and Information Technologies (ICEIT)* (pp. 84-88). IEEE.
- [22] Gaillard, A. (2010). *Système éolien basé sur une MADA : contribution à l'étude de la qualité de l'énergie électrique et de la continuité de service* (Doctoral dissertation, Université Henri Poincaré-Nancy 1).
- [23] Yang, L., Xu, Z., Ostergaard, J., Dong, Z. Y., & Wong, K. P. (2011). Advanced control strategy of DFIG wind turbines for power system fault ride through. *IEEE Transactions on power systems*, 27(2), 713-722.
- [24] Boukhezzer, B., Lupu, L., Siguerdidjane, H., & Hand, M. (2007). Multivariable control strategy for variable speed, variable pitch wind turbines. *Renewable Energy*, 32(8), 1273-1287.